Quantum tunneling in dispersive optical bistability

H. Risken,* C. Savage, F. Haake,† and D. F. Walls

Physics Department, University of Waikato, Hamilton, New Zealand

(Received 23 June 1986)

Quantum tunneling times for the model of Drummond and Walls describing dispersive optical bistability are investigated for small cavity damping. Without damping the system can be described by an appropriate Hamilton operator. By expanding the density operator in eigenstates of this Hamilton operator the stationary solution as well as the lowest eigenvalues are obtained from a Pauli master equation for the diagonal elements of the density matrix for small cavity damping. The tunneling time follows from the lowest nonzero eigenvalue of this master equation. Expectation values as well as the Q function for the stationary case are also presented.

I. INTRODUCTION

In optical bistability, as in every bistable system, one has two nearly stable states. (For a recent review article on optical bistability, see Ref. 1.) Without any fluctuations no transitions between these two states are possible. If, however, fluctuations are taken into account one has a certain probability that the system jumps from one state to the other. The simplest example is the classical Brownian motion of a particle in a double-well potential. Due to thermal excitations the particle in one well may sometimes accumulate enough energy to cross the barrier between the wells and thus move to the other well. In his pioneering work Kramers[2] treated this problem and especially calculated the escape time for this system. For a quantum particle a transition out of one well may occur even without thermal fluctuations. It is only necessary that the wave function penetrates through the potential barrier. This quantum tunneling in the presence of an additional damping term is the topic of recent theoretical[3-6] and experimental research.[7]

For absorptive optical bistability, escape times have been calculated by Lugiato and co-workers (see Sec. 3.6 of Ref. 1 for a review) and by Schenzle and Brand.[8] In Ref. 1 the escape time is obtained from a suitable Fokker-Planck equation with a fixed phase using essentially the Kramers method. In Ref. 8 a variational method is used to obtain the lowest nonzero eigenvalue of the Fokker-Planck equation with the inclusion of the phase. The lowest nonzero eigenvalue determines the escape time. Drummond[9] has remarked that various representations of the density operator, i.e., P and Q functions lead to different Fokker-Planck equations which in turn lead to very different escape times. In his paper Drummond also calculates escape times for dispersive optical bistability. Because of the adiabatic approximation made in,[9] however, his result is only valid near the turning points of the output field versus input field plot without fluctuations.

In the present paper we calculate the tunneling time numerically for the model of Drummond and Walls[10] describing dispersive optical bistability. In this model one has transitions between the bistable states even for temperature $T=0$. Thus the fluctuations causing the transi-

tion for $T=0$ are pure quantum fluctuations. The tunneling time is obtained from eigenvalues of the density operator equation for the system. In the bistable region one of the eigenvalues becomes very small. This eigenvalue then determines the tunneling time. The density operator equation consists of a reversible part with a system Hamilton operator and the irreversible part describing the cavity damping. The essential assumption in our procedure is a small cavity damping. Expanding the density operator in eigenstates of the system Hamilton operator the lowest eigenvalue then follows from the Pauli master equation for the diagonal elements of the density operator. As we will show, we are able to determine the lowest nonzero eigenvalue as well as some other low eigenvalues in and outside the bistable region. In Ref. 10 the density operator equation was transformed to a Fokker-Planck equation for the complex P function.[11] Because detailed balance is valid, the complex P function was obtained analytically for the stationary state. In the present procedure the stationary solution is also obtained from the Pauli master equation. To check the present procedure stationary results following from the present procedure are compared with the analytic results of Ref. 10.

The present paper is organized as follows. In Sec. II the model and the basic equations are presented. In Sec. III the classical equations without quantum fluctuations are given. Next, in Sec. IV the eigenvalues and eigenfunctions of the system Hamilton operator are calculated. In Sec. V the density operator is expanded into eigenstates of the system Hamilton operator leading to a Pauli master equation for the diagonal elements. In Sec. VI the stationary solutions of this master equation, some expectation values and the Q function are presented. In Sec. VIII the eigenvalues as a function of the driving field are plotted and the connection to the tunneling times is given.

II. MODEL AND BASIC EQUATIONS

A quantum theory for a nonlinear polarization model describing dispersive optical bistability was developed by Drummond and Walls[10] some time ago. The main ingredients of their model are

(i) expanding the polarization up to third order,
(ii) including a coherent classical driving field,
(iii) adding losses due to cavity damping, and
(iv) making the rotating-wave approximation.

In this way they obtained the following master equation for the density operator ρ for the light field inside the cavity:

$$\dot{\rho} = \sum_{j=1}^{4} L_j[\rho] \ ,$$

$$L_1[\rho] = -i\Delta\omega[a^\dagger a, \rho] \ ,$$

$$L_2[\rho] = -i\chi''[a^{\dagger 2} a^2, \rho], \qquad (2.1)$$

$$L_3[\rho] = [(Ea - E^* a^\dagger), \rho] \ ,$$

$$L_4[\rho] = \kappa'(2a\rho a^\dagger - \rho a^\dagger a - a^\dagger a \rho + 2n_{\text{th}}[[a,\rho], a^\dagger]) \ .$$

Here $a^\dagger$ and a are the creation and annihilation operators of the light field, $\Delta\omega = \omega_c - \omega_l$ is the difference between the cavity frequency ω_c and the frequency ω_1 of the classical driving light field E, χ'' is the imaginary part of the third-order susceptibiilty, κ' is the cavity damping constant, and n_{th} the number of thermally excited optical quanta. As shown in Ref. 12, the last term in the above master equation has to be modified for high temperatures. Because we treat the zero-temperature limit ($n_{\text{th}} = 0$), in the results of Secs. VI and VII this modification is not important in the final results derived in this paper. As already mentioned in the introduction, for the stationary state equation (2.1) was solved in Ref. 10 by using the complex P function (see Chap. 10.6 of Ref. 11 for further details of a complex P function). In this way a Fokker-Planck equation for the two complex variables of the P function was derived. As it was further shown in Ref. 10 the potential conditions are valid for this Fokker-Planck equation and therefore analytic expression was given. The stationary expectation values were obtained in terms of hypergeometric series. For calculating tunneling times numerically the Fokker-Planck equation for the complex P function seems to be not very useful because of the large number of variables (two independent complex ones equal four real ones). As shown in Sec. VII we calculate the tunneling time without using the complex P function.

Equation (2.1) can be written in the form

$$\dot{\rho} = i[H, \rho] + \kappa L_{ir}[\rho] \ , \qquad (2.2)$$

$$H = -\Omega a^\dagger a + \chi a^{\dagger 2} a^2 - F(a + a^\dagger) \ , \qquad (2.3)$$

$$L_{ir}[\rho] = 2a\rho a^\dagger - \rho a^\dagger a - a^\dagger a \rho + 2n_{\text{th}}[[a,\rho], a^\dagger] \ , \qquad (2.4)$$

with

$$\Omega = -\Delta\omega, \quad \chi = \chi'', \quad \kappa = \kappa', \quad F = -iE \ . \qquad (2.5)$$

Here Ω, χ, κ are used instead of $-\Delta\omega, \chi'', \kappa'$ for convenience of notation, the last equation with real F in (2.5) fixes the phase of the driving field E.

The first part on the right-hand side of (2.2) describes the coherent motion of the density operator, the second part the irreversible motion of it.

III. CLASSICAL EQUATION WITHOUT FLUCTUATIONS

From the density operator equations (2.2) and (2.3) without the damping terms we obtain for the amplitude

$$\alpha = \text{Tr}(a\rho), \quad \alpha^* = \text{Tr}(a^\dagger \rho) \qquad (3.1)$$

the equation

$$\dot{\alpha} = i\Omega\alpha - 2i\chi \, \text{Tr}(a^\dagger a^2 \rho) + iF \ . \qquad (3.2)$$

According to the classical assumption we replace the expectation values of the operators $a^\dagger a^2$ by the expectation values of the amplitudes (3.1), i.e.,

$$\text{Tr}(a^\dagger a^2 \rho) = \alpha^* \alpha^2 \qquad (3.3)$$

and thus arrive at

$$\dot{\alpha} = i\Omega\alpha - 2i\chi\alpha^*\alpha\alpha + iF \ . \qquad (3.4)$$

For $F \neq 0$ (3.4) has the stationary solutions

$$\alpha^{\text{st}} = x^{\text{st}} + iy^{\text{st}} \ , \qquad (3.5)$$

$$y^{\text{st}} = 0, \quad F = -\Omega x^{\text{st}} + 2\chi (x^{\text{st}})^3 \ . \qquad (3.6)$$

For $\Omega > 0$ it is easily shown that the solution (3.6) is stable for

$$(x^{\text{st}})^2 < \Omega/(6\chi)$$

or

$$(x^{\text{st}})^2 > \Omega/(2\chi) \qquad (3.7)$$

and unstable for

$$\Omega/(6\chi) < (x^{\text{st}})^2 < \Omega/(2\chi) \ .$$

The stable and unstable stationary solutions of (3.4) are plotted in Fig. 1. For $\Omega \leq 0$ (3.4) possesses only one stable solution.
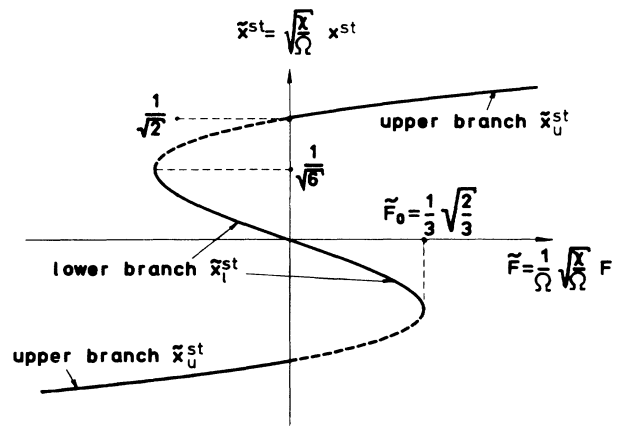

FIG. 1. Stationary values x^{st} as a function of the driving field F according to (3.6). The corresponding normalized quantities of (3.8) are marked by a tilde. Solid line: stable stationary solutions. Broken line: unstable stationary solutions.

Normalization

By using the normalized time $\tilde{t}$, amplitude $\tilde{\alpha}$, and driving field $\tilde{F}$ defined by ($\Omega > 0$)

$$\tilde{t} = \Omega t, \quad \tilde{\alpha} = \sqrt{X/\Omega}\,\alpha, \quad \tilde{F} = (1/\Omega)\sqrt{X/\Omega}\,F \qquad (3.8)$$

(3.4) is transformed to the normalized form

$$d\tilde{\alpha}/d\tilde{t} = i\tilde{F} + i\tilde{\alpha}(1 - 2\tilde{\alpha}^*\,\tilde{\alpha}) , \qquad (3.9)$$

i.e., one obtains the same equation for every X, F, $\Omega > 0$. Because the intensity $I = \alpha^*\alpha$ scales according to

$$I = (\Omega/X)\tilde{I} , \qquad (3.10)$$

a large parameter ratio Ω/X leads to high photon numbers, i.e., to a nearly classical behavior.

IV. EIGENVALUES AND EIGENFUNCTIONS OF THE HAMILTON OPERATOR

The eigenvalues E_m and the eigenstates $|m\rangle$ of the Hamilton operator (2.3)

$$H\,|m\rangle = E_m\,|m\rangle \qquad (4.1)$$

are calculated by expanding the eigenstates $|m\rangle$ into Fock states $|n\rangle$

$$|m\rangle = \sum_{n=0}^{\infty} c_{m,n}\,|n\rangle . \qquad (4.2)$$

Insertion of (2.3) into (4.1) and using

$$a^\dagger a\,|n\rangle = n\,|n\rangle ,$$
$$a\,|n\rangle = \sqrt{n}\,|n-1\rangle , \qquad (4.3)$$
$$a^\dagger\,|n\rangle = \sqrt{n+1}\,|n+1\rangle$$

we easily obtain the following tridiagonal recurrence relation for the expansion coefficients $c_{m,n}$

$$F\sqrt{n+1}\,c_{m,n+1} + [E_m + \Omega n - Xn(n-1)]c_{m,n}$$
$$+ F\sqrt{n}\,c_{m,n-1} = 0 . \qquad (4.4)$$

Because of the tridiagonal structure the normalized real eigenvectors $c_{m,n}$, i.e.,

$$\sum_{n=0}^{\infty} c_{m,n}c_{m',n} = \delta_{m,m'} \qquad (4.5)$$

and eigenvalues E_m can easily be determined by using a suitable computer subprogram for tridiagonal matrices. The eigenvalues also follow as roots of the continued fraction

$$D(E) = -E - \frac{1F^2}{-1\Omega - E} - \frac{2F^2}{-2\Omega + 1 \times 2X - E}$$
$$- \frac{3F^2}{-3\Omega + 2 \times 3X - E} - \cdots . \qquad (4.6)$$

The eigenvector can be obtained by using a stable up iteration, see, for instance, Sec. IX of Ref. 13 for a summary and further applications of the continued fraction method. The eigenvalues E_m as a function of the driving field are shown in Fig. 2.
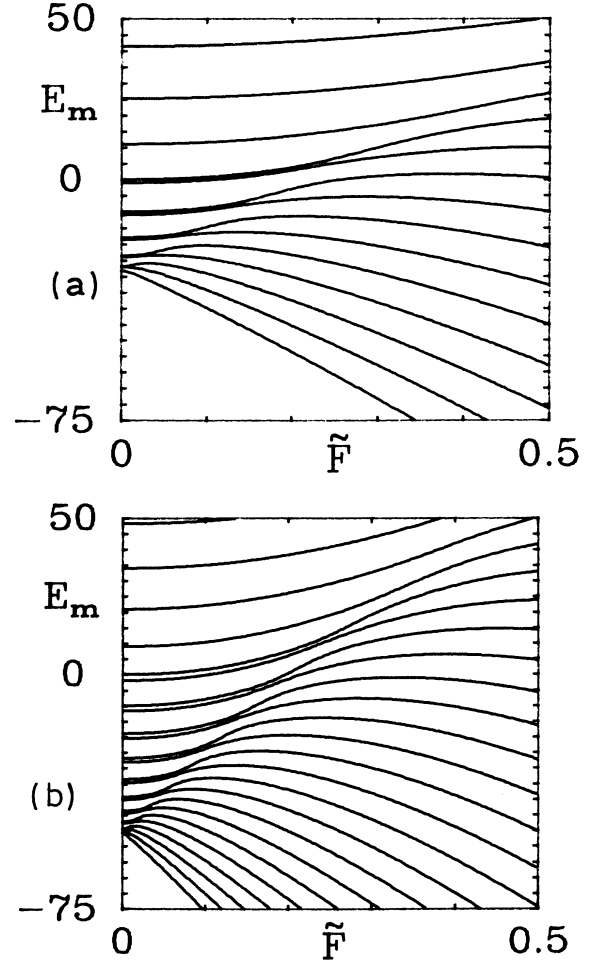

FIG. 2. Eigenvalues of the Hamilton operator (2.3) as a function of the normalized field (3.8) for $X = 1.1$ (a), $X = 0.55$ (b), and $\Omega = 10$.

For zero field, eigenvalues and normalized eigenvectors are given by the analytic expression

$$E_m = -\Omega m + Xm(m-1), \quad c_{m,n} = \delta_{m,n} . \qquad (4.7)$$

If Ω/X is an integer number the eigenvalues are degenerate

$$E_{m_1} = E_{m_2} \quad \text{for} \quad m_1 + m_2 = 1 + \Omega/X, \quad m_1 \geqq 0, \quad m_2 \geqq 0 . \qquad (4.8)$$

For $F \neq 0$ this degeneracy is lifted. As seen in Fig. 2 the differences of the eigenvalues increase with increasing F.

For the parameters in Fig. 2 the expansion (4.2) was truncated at $n = 50$. Because of this truncation we cannot treat the problem for very large Ω/X ratios, i.e., for very large photon numbers. It turns out that the number of states which have to be included for properly treating the ground state, must be about 2.5 times larger than Ω/X.

For an approximate expression of the lowest eigenvalue, see the Appendix.

Matrix elements

In the derivation of the Pauli master equation in Sec. V we need the matrix elements

$$(m \mid a \mid l) = (l \mid a^\dagger \mid m) = \sum_{n=0}^{\infty} \sqrt{n+1} c_{m,n} c_{l,n+1} ,$$

$$(m \mid a^\dagger a \mid m) = \sum_{n=1}^{\infty} n c_{m,n}^2 . \tag{4.9}$$

As seen from (4.9) they follow immediately from the normalized eigenvectors $c_{m,n}$. For the calculation of $g_2(0)$ in (6.4) we also need the matrix element

$$(m \mid a^{\dagger 2} a^2 \mid m) = (m \mid [(a^\dagger a)^2 - a^\dagger a] \mid m)$$

$$= \sum_{n=2}^{\infty} n(n-1) c_{m,n}^2 . \tag{4.10}$$

V. EXPANSION OF THE DENSITY OPERATOR

For vanishing κ the system will remain for ever in an eigenstate of H if it was initially in such a state. If κ is small but finite the irreversible term in (2.2) determines the occupation number of that state. For small κ the best way to solve (2.2) seems to be to expand the density operator ρ into eigenstates $\mid m)$ of the Hamilton operator H, i.e.,

$$\rho = \sum_{m,p} \mid m) \rho_{mp}(p \mid , \quad \rho_{mp} = (m \mid \rho \mid p) . \tag{5.1}$$

Insertion of (5.1) into (2.2) with H and $\mathbf{L}_{ir}$ given by (2.3) and (2.4) leads to

$$\dot{\rho}_{mp} = -i(E_m - E_p)\rho_{mp} + \kappa \sum_{q,r} M_{mpqr}\rho_{qr} , \tag{5.2}$$

$$M_{mpqr} = 2(m \mid a \mid q)(p \mid a \mid r) - (p \mid a^\dagger a \mid r)\delta_{mq}$$

$$- (m \mid a^\dagger a \mid q)\delta_{pr}$$

$$+ 2n_{th}[(m \mid a \mid q)(p \mid a \mid r) + (m \mid a^\dagger \mid q)(p \mid a^\dagger \mid r)$$

$$- (p \mid aa^\dagger \mid r)\delta_{mq} - (m \mid a^\dagger a \mid q)\delta_{pr}] . \tag{5.3}$$

We now want to restrict ourselves to the slow motion of the density operator ρ (time scale of the order $1/\kappa$). Then $\dot{\rho}_{mp}$ is of the order $\kappa\rho_{mp}$. Furthermore, it follows from the nondiagonal elements of (5.2) that the nondiagonal elements $m \neq p$ are of the order

$$\mid \rho_{mp} \mid = \mathcal{O}(\kappa / \mid E_m - E_p \mid)\mathcal{O} \text{ (diagonal elements) .} \tag{5.4}$$

Therefore we can also neglect the off-diagonal elements in the right-hand side of (5.2) for the equations with $m = p$ if κ is much smaller than the differences between the eigenvalues E_m. Introducing the occupation probability p_m of the state $\mid m)$

$$p_m = \rho_{mm} \tag{5.5}$$

we thus obtain for p_m the Pauli master equation

$$\dot{p}_m = 2\kappa \left[\sum_l w(l \rightarrow m)p_l - \sum_l w(m \rightarrow l)p_m \right]$$

$$= 2\kappa \sum_l W_{ml}p_l , \tag{5.6}$$

where the matrix W_{ml} is given by

$$W_{ml} = \mid (m \mid a \mid l) \mid^2 (1 + n_{th}) + \mid (m \mid a^\dagger \mid l) \mid^2 n_{th}$$

$$- [(m \mid a^\dagger a \mid m)(1 + n_{th}) + (m \mid aa^\dagger \mid m)n_{th}]\delta_{ml} . \tag{5.7}$$

The transition probabilities $w(l \rightarrow m)$ in (5.6) read

$$w(l \rightarrow m) = \mid (m \mid a \mid l) \mid^2 (1 + n_{th}) + \mid (m \mid a^\dagger \mid l) \mid^2 n_{th} . \tag{5.8}$$

In order to verify the first part of (5.6) and

$$\sum_m W_{ml} = 1 \tag{5.9}$$

one has to use

$$\sum_l \mid (l \mid a \mid m) \mid^2 = \sum_l (m \mid a^\dagger \mid l)(l \mid a \mid m)$$

$$= \left[m \left| a^\dagger \sum_l \right| l \right] (l \mid a \mid m)$$

$$= (m \mid a^\dagger a \mid m) \tag{5.10}$$

and a similar expression for $\sum_l \mid (l \mid a^\dagger \mid m) \mid^2$. With the numerical procedure described in Sec. IV it is an easy matter to obtain the transition probabilities $w(l \rightarrow m)$ and the transition matrix W_{ml}.

The stationary solution of (5.6) could easily be obtained if detailed balance would be valid, i.e.,

$$w(l \rightarrow m)p_l^{st} = w(m \rightarrow l)p_m^{st} . \tag{5.11}$$

A numerical check with the stationary solution showed, however, that the detailed balance condition (5.11) is not valid for driving fields different from zero.

In the results of the following two sections we have neglected the number of thermal quanta n_{th} in (5.6) and (5.7).

VI. RESULTS FOR THE STATIONARY STATE

Though our main aim in this paper is the determination of the tunneling times, it seems to be appropriate to calculate stationary solutions and expectation values with our procedure as well. Firstly, a comparison with the analytical results of Ref. 10 gives a check of the presented method. Secondly, it will lead to the conclusion that for the damping constant used in Ref. 10 our low-damping-constant procedure is already very well applicable. Therefore the calculation of the tunneling times should work for this damping constant also very well.

The stationary solution of (5.6) is obtained by calculating the eigenvector of the matrix W_{ml} belonging to the stationary eigenvalue $\lambda_{st} = 0$. (Because of $\sum_{m=0}^{\infty} W_{ml} = 0$ a stationary solution must always exist, see Ref. 14.) For the calculation of the results in the present paper it was
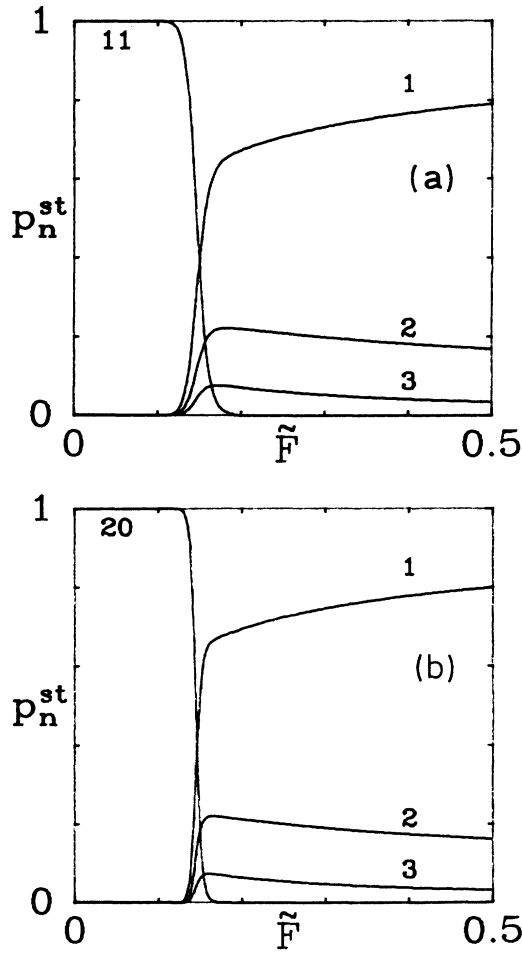
FIG. 3. The stationary solutions of the master equation (5.6) as a function of the normalized field (3.8) for $\chi = 1.1$ (a), $\chi = 0.55$ (b), and $\Omega = 10$.

sufficient to use the first 50×50 matrix elements of W_{ml}. In Fig. 3 the stationary occupation probability is shown as a function of the driving field for two typical values of Ω / χ. The remarkable feature is that for fields $|F|$ smaller than a transition field F_{tr} ($\tilde{F}_{\text{tr}} \approx 0.142$) the occupation probability for that state which evolves from the vacuum state for $F = 0$ is nearly one. In Figs. 3(a) and 3(b) the number of this state is 11 or 20, respectively. Then at F_{tr} a sudden change occurs. For fields $|F|$ larger than F_{tr} the occupation probability of the lowest energy state (number 1) of H is maximal and only the next energy states 2 and 3 have an appreciable probability. The sum of p_1, p_2, and p_3 is approximately 1. For increasing $\tilde{F}$ the probability of p_1 is slowly increasing to 1 whereas p_2 and p_3 slowly decrease to zero. For the larger values of Ω / χ in Fig. 3(b) (larger photon numbers) the transition is more abrupt than in Fig. 3(a) for the lower value of Ω / χ.

A. Stationary expectation values

The expectation values of the amplitude $\langle a \rangle$, of the intensity $\langle a^\dagger a \rangle$ and of the second-order correlation func-

tion at $\tau = 0$ follow from

$$\rho = \sum_m p_m^{\text{st}} |m\rangle\langle m| \ , \tag{6.1}$$

i.e.,

$$\langle a \rangle = \sum_m p_m^{\text{st}} \langle m | a | m \rangle \ , \tag{6.2}$$

$$\langle a^\dagger a \rangle = \sum_m p_m^{\text{st}} \langle m | a^\dagger a | m \rangle \ , \tag{6.3}$$

$$g_2(0) = \frac{\langle a^\dagger a^\dagger a a \rangle}{\langle a^\dagger a \rangle^2} = \frac{\sum_m p_m^{\text{st}} \langle m | a^{\dagger 2} a^2 | m \rangle}{\left[\sum_m p_m^{\text{st}} \langle m | a^\dagger a | m \rangle \right]^2} \ . \tag{6.4}$$

The procedure for calculating the matrix elements occurring in (6.2)–(6.4) is explained in Sec. IV, see (4.9) and (4.10). In Fig. 4 the amplitude $\langle a \rangle$ is shown as a function of the driving field F. Below the transition field F_{tr} the expectation value nearly agrees with the classical lower stable branch (see Fig. 1). At F_{tr} one has again an
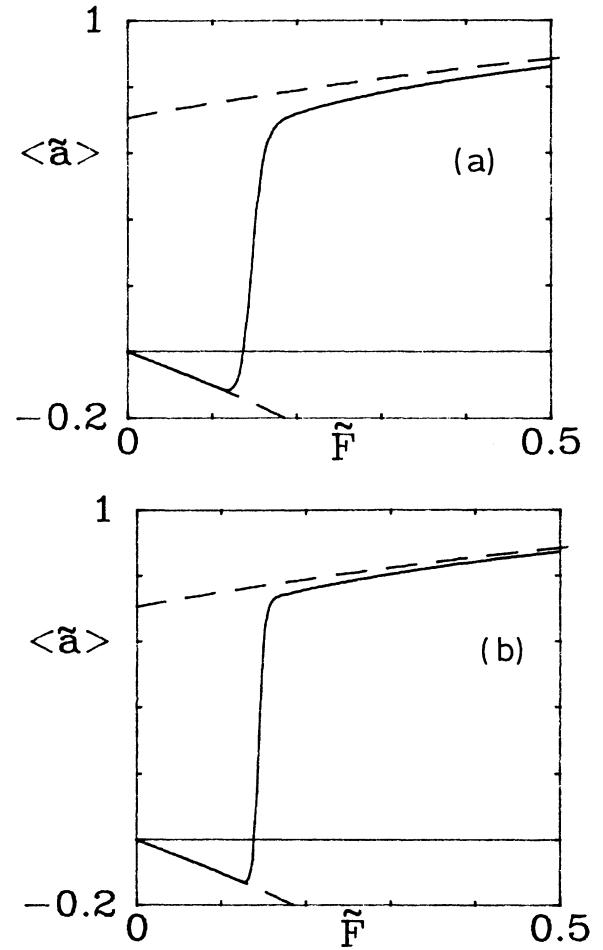

FIG. 4. The averaged normalized amplitude $\tilde{a} = \langle \tilde{a} \rangle$ as a function of the normalized field [see (3.8) for the normalization] for $\chi = 1.1$ (a), $\chi = 0.55$ (b), and $\Omega = 10$ (solid line). The classical result according to Fig. 1 is shown by a broken line.

abrupt change and for $| F |$ larger than F_{tr} the curve approximately agrees with the classical upper branch of Fig. 1. For the larger value $\Omega/X = 0.55$ in Fig. 4(b) the transition is more abrupt and it better coincides with the classical curve than for the lower value $\Omega/X = 10/1.1$ in Fig. 4(a). Comparing Fig. 4(b) with the result of Fig. 1 of Ref. 10, $| \langle a \rangle |$ nearly agrees with the corresponding curve in Fig. 1 of Ref. 10. The small discrepancies occur because Fig. 1 of Ref. 10 is calculated with a finite κ. If in (5.17) of Ref. 10 κ is made very small, both results agree within the accuracy of the plot. In Fig. 5(a) and 5(b) the intensity $\langle a^{\dagger}a \rangle$ and the amplitude squared $| \langle a \rangle |^2$ is plotted. Both curves approximately agree for driving fields below and above the transition field, near the transition field F_{tr}, however, the deviations become very large. This means of course that near F_{tr} the problem cannot be treated by the classical equations, outside this transition region the classical results for the lower branch ($| F | < F_{tr}$) and for the upper branch ($| F | > F_{tr}$) lead to very good approximations for the stationary expectation values. The agreement is better in Fig. 5(b) than in Fig. 5(a) because we
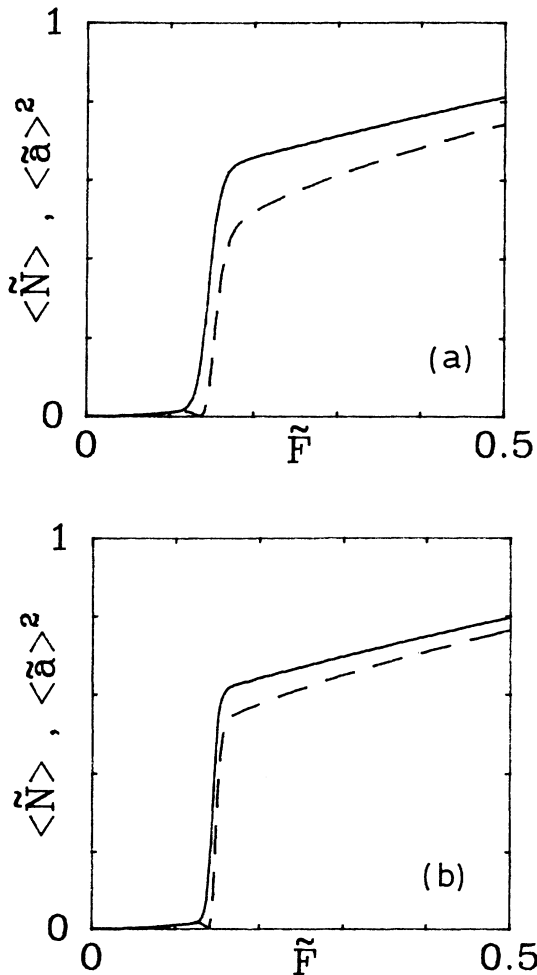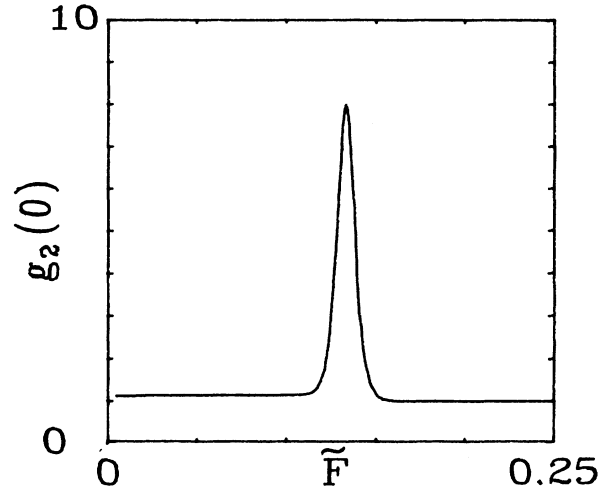

FIG. 6. The correlation function (6.4) as a function of the normalized field $\tilde{F}$ for $\Omega = 10$ and $X = 0.55$.

have the larger value of Ω/X in Fig. 5(b).

The correlation function $g_2(0)$ is shown in Fig. 6 as a function of the driving field. As seen one gets a high peak [variance is $g_2(0) - 1$] at the transition field $F \approx F_{tr}$.

B. Determination of the Q function

Because of a possible squeezing of the field amplitude[15] the Glauber-Sudarshan P function does not always exist. The Q function, however, does. It is defined by

$$Q(\alpha) = \langle \alpha | \rho | \alpha \rangle \ , \tag{6.5}$$

where $| \alpha \rangle$ is the coherent state. The Q function is positive everywhere. Every antinormally ordered expectation value can be evaluated with the help of the Q function according to

$$\langle a^n a^{\dagger m} \rangle = \frac{1}{\pi} \int \alpha^n \alpha^{*m} Q(\alpha) d^2\alpha \ . \tag{6.6}$$

Because of (6.1) we have

$$Q(\alpha) = \sum_m p_m^{st} | \langle \alpha | m \rangle |^2 \ . \tag{6.7}$$

Using (4.2) and

$$\langle \alpha | n \rangle = \frac{\alpha^{*n}}{\sqrt{n!}} e^{-|\alpha|^2/2} \tag{6.8}$$

we obtain for the matrix elements

$$| \langle \alpha | m \rangle |^2 = \sum_{n,n'} c_{m,n} c_{m,n'} \frac{\alpha^n \alpha^{*n'}}{(n!n'!)^{1/2}} e^{-|\alpha|^2} \ . \tag{6.9}$$

The contour lines of the Q function in the complex α plane for four typical driving fields are shown in Fig. 7. If $| F |$ is smaller than the transition field F_{tr} we have approximately a Gaussian distribution with circular symmetry centered around $\alpha_l = x_l^{st}$ where x_l^{st} is the solution of the classical equation for the lower branch

FIG. 5. The normalized intensity (solid line) and the amplitude squared (broken line) as a function of the normalized field F for $X = 1.1$ (a), $X = 0.55$ (b), and $\Omega = 10$.
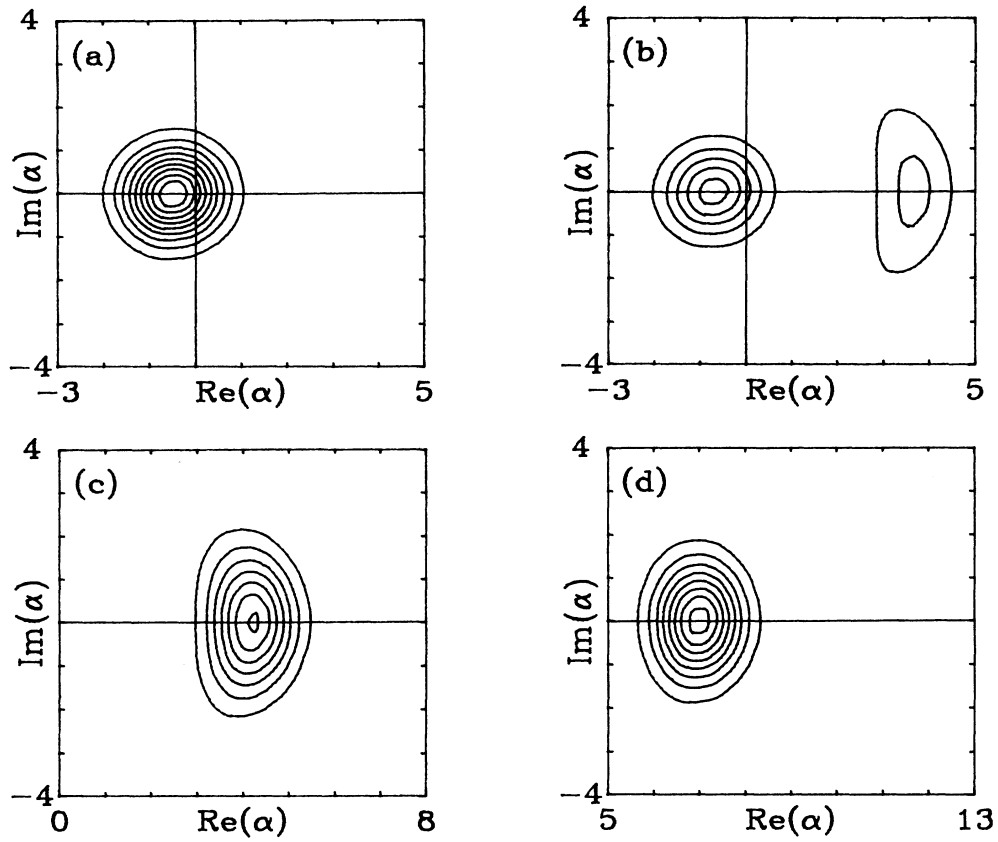
FIG. 7. Contour lines of the $Q(\alpha)$ function (6.5) for the normalized forces $\tilde{F}=0.1$ (a), $\tilde{F}=0.142$ (b), $\tilde{F}=0.5$ (c), $\tilde{F}=5.0$ (d), and for $\Omega=10$, $\chi=0.55$. The contour lines start at $Q=0.1$ [outermost line in (a), (c), (d) or lines in (b)] and have a separation of $\Delta Q=0.1$.
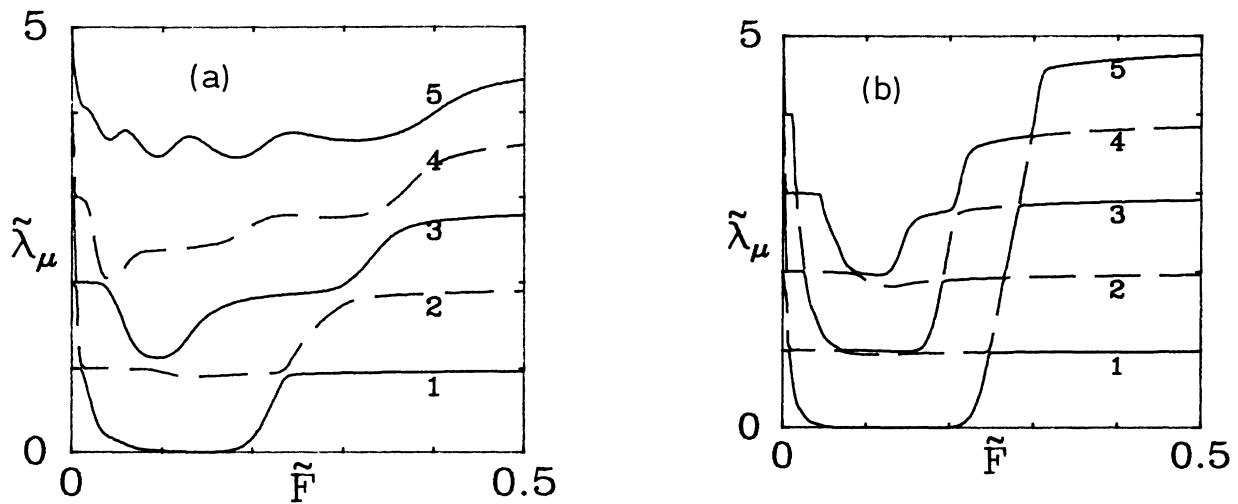
FIG. 8. The five lowest nonzero eigenvalues $\tilde{\lambda}_\mu$ of the matrix (5.7) for $\chi=1.1$ (a), $\chi=0.55$ (b), $n_{\rm th}=0$ and $\Omega=10$ as a function of the normalized field $\tilde{F}$.

$$Q(\alpha) \approx e^{-|\alpha - x_l^{st}|^2} , \qquad (6.10)$$

i.e., the system is approximately in the coherent state

$$\rho \approx |\alpha_l\rangle\langle\alpha_l| . \qquad (6.11)$$

In the transition region another peak appears centered approximately at x_u^{st}, where x_u^{st} is the upper branch of the classical solution in Fig. 1. Instead of having a circular symmetry the contour lines of the right peak are earshaped. For driving fields in the transition region, where one has two peaks as in Fig. 7(b), the variance has, of course, a very large value, compare Fig. 6. For larger fields the left peak disappears and the contour lines are of an elliptical shape. By comparing Figs. 7(c) and 7(d) there is the indication that even for larger driving fields one again gets a circular symmetry. The variance in the real quadrature phase $(a + a^\dagger)/2$ is obviously smaller than in the imaginary phase $(a - a^\dagger)/(2i)$ for larger driving fields.

VII. EIGENVALUES AND TUNNELING TIME

If the energy differences $E_m - E_p$ of the Hamilton operator (2.3) are much larger than the cavity damping constant κ the low eigenvalues of the density operator equation (2.2) are given by the eigenvalues λ of the Pauli
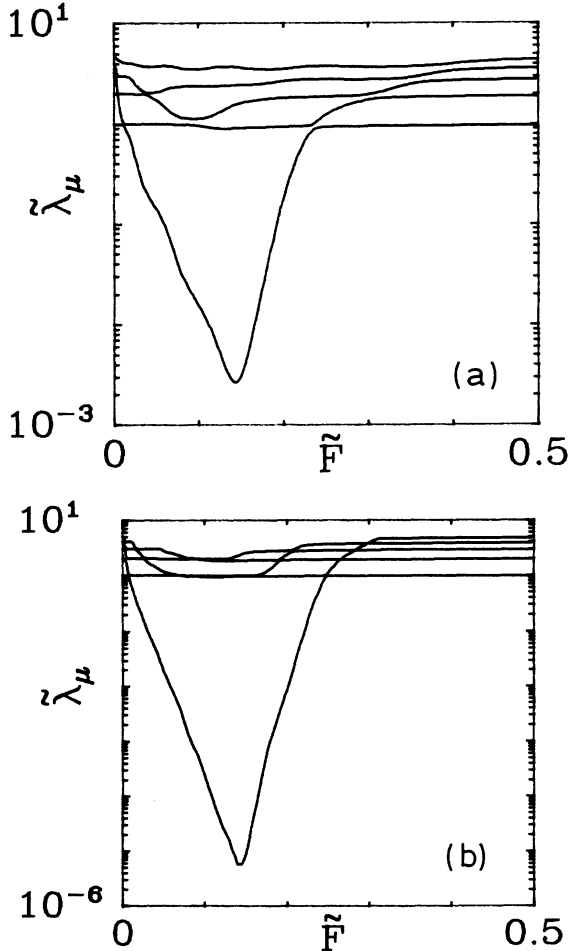

(a)

(b)

FIG. 9. Logarithmic plot of the eigenvalues of Fig. 8.

master equation (5.6) for the diagonal elements of the density operator. These in turn are given by the negative eigenvalues $\tilde{\lambda}_\mu$ of the matrix W_{ml} multiplied with 2κ, i.e.,

$$\lambda = 2\kappa\tilde{\lambda}_\mu , \qquad (7.1)$$

$$\sum_l W_{ml}\,\hat{p}\,_l^{(\mu)} = -\tilde{\lambda}_\mu\hat{p}\,_m^{(\mu)} . \qquad (7.2)$$

The eigenvalues $\tilde{\lambda}_\mu$ are shown in Figs. 8 and 9 as a function of the driving field F. In the bistability region $0 < |\tilde{F}| < \tilde{F}_0 = 0.2722$ the lowest nonzero eigenvalue becomes very small. Furthermore, it is very well separated from the other larger ones. It reaches its lowest value near the transition field F_{tr} as best seen from the logarithmic plots in Fig. 9. The lowest nonzero eigenvalue reaches lower values for the larger Ω/χ parameter as seen by comparing Figs. 9(a) and 9(b).

A. Connection to the tunneling time

The lowest nonzero eigenvalue is connected to the tunneling time of the transition from the lower branch to the upper branch of the semiclassical curve in Fig. 1 and vice versa. This can be seen as follows. The matrix elements of the amplitude of the states with the lowest eigenvalue, i.e., $(1 | a | 1)$, $(2 | a | 2)$, and $(3 | a | 3)$ are nearly equal to the amplitude x_u^{st} of the classical upper branch whereas the matrix element of the amplitude for the state which had evolved for $F = 0$ from the vacuum state, i.e., $(11 | a | 11)$ and $(20 | a | 20)$ for the parameters of Figs. 3(a) and 3(b), is nearly equal to the amplitude x_l^{st} of the classical lower branch. Thus the probabilities to find the system in the upper (u) or lower (l) branch are given by

$$p_u \approx p_1 + p_2 + p_3 ,$$

$$p_l \approx p_{11} , \qquad (7.3)$$

$$p_l \approx p_{22} ,$$

see Fig. 3(a) for p_{11} and 3(b) for p_{22}. The time-dependent probabilities $p_m(t)$ and therefore also $p_u(t)$ and $p_l(t)$ can be expanded into eigenstates $\hat{p}\,_m^{(\mu)}$ of the matrix W_{ml},

$$p_m(t) = p_m^{st} + \sum_{\mu=1}^{\infty} c^{(\mu)}\hat{p}\,_m^{(\mu)}e^{-2\kappa\tilde{\lambda}_\mu t} , \quad m = 1,2,3,\ldots ,$$

$$p_u(t) = p_u^{st} + \sum_{\mu=1}^{\infty} c^{(\mu)}\hat{p}\,_u^{(\mu)}e^{-2\kappa\tilde{\lambda}_\mu t} , \qquad (7.4)$$

$$p_l(t) = p_l^{st} + \sum_{\mu=1}^{\infty} c^{(\mu)}\hat{p}\,_l^{(\mu)}e^{-2\kappa\tilde{\lambda}_\mu t} .$$

Here the constants $c^{(\mu)}$ depend on the initial conditions. The $\hat{p}\,_u^{(\mu)}$ and $\hat{p}\,_l^{(\mu)}$ are connected to the eigenvectors $\hat{p}\,_m^{(\mu)}$ according to (7.3).

If we wait until all the exponentials with the exception of the first one have vanished [i.e., $\exp(-2\kappa\tilde{\lambda}_2 t) \ll 1$] the solutions for p_u and p_l read

$$p_u(t) = p_u^{st} + c^{(1)}\hat{p}\,_u^{(1)}e^{-2\kappa\tilde{\lambda}_1 t} ,$$

$$p_l(t) = p_l^{st} + c^{(1)}\hat{p}\,_l^{(1)}e^{-2\kappa\tilde{\lambda}_1 t} . \qquad (7.5)$$

Some of the eigenvectors $\hat{p}_m^{(1)}$ are plotted in Fig. 10. As is seen in this figure $\hat{p}_u^{(1)}$ and $\hat{p}_l^{(1)}$ are approximately given by

$$\hat{p}_u^{(1)} \approx 1, \quad \hat{p}_l^{(1)} \approx -1 \tag{7.6}$$

in the bistability region. It follows from (7.5) and (7.6) that $p_u(t)$ and $p_l(t)$ obey the two-state master equation

$$\dot{p}_u = -w(u \to l)p_u + w(l \to u)p_l \ ,$$

$$\dot{p}_l = w(u \to l)p_u - w(l \to u)p_l \ , \tag{7.7}$$

where the transition rates from the upper to the lower branch and vice versa are given by

$$w(u \to l) = 2\kappa \tilde{\lambda}_1 p_l^{st} \ ,$$

$$w(l \to u) = 2\kappa \tilde{\lambda}_1 p_u^{st} \ . \tag{7.8}$$

The tunneling times from the upper to the lower branch and vice versa are the inverse rates, i.e.,

$$T(u \to l) = 1/w(u \to l), \quad T(l \to u) = 1/w(l \to u) \ . \tag{7.9}$$

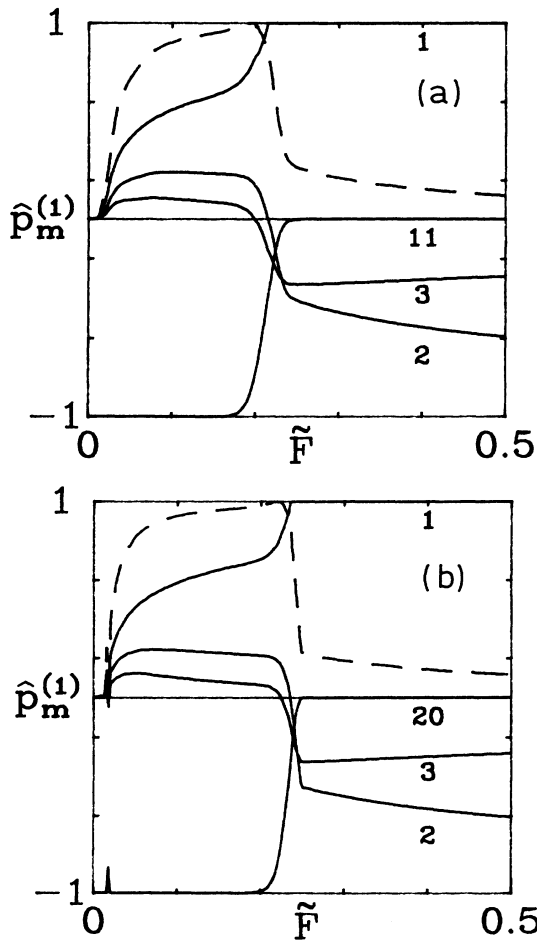The rates $w(u \to l)/2\kappa$ and $w(l \to u)/2\kappa$ are plotted in

FIG. 10. The eigenvector $\hat{p}_m^{(1)}$ of the matrix W_{ml} with the lowest nonzero eigenvalue $\tilde{\lambda}_1$ as a function of the normalized field $\tilde{F}_1$ for $\chi = 1.1$ (a), $\chi = 0.55$ (b), and $\Omega = 10$ (solid lines). The sum $\hat{p}_u^{(1)} = \hat{p}_1^{(1)} + \hat{p}_2^{(1)} + \hat{p}_3^{(1)}$ is also shown (broken line).
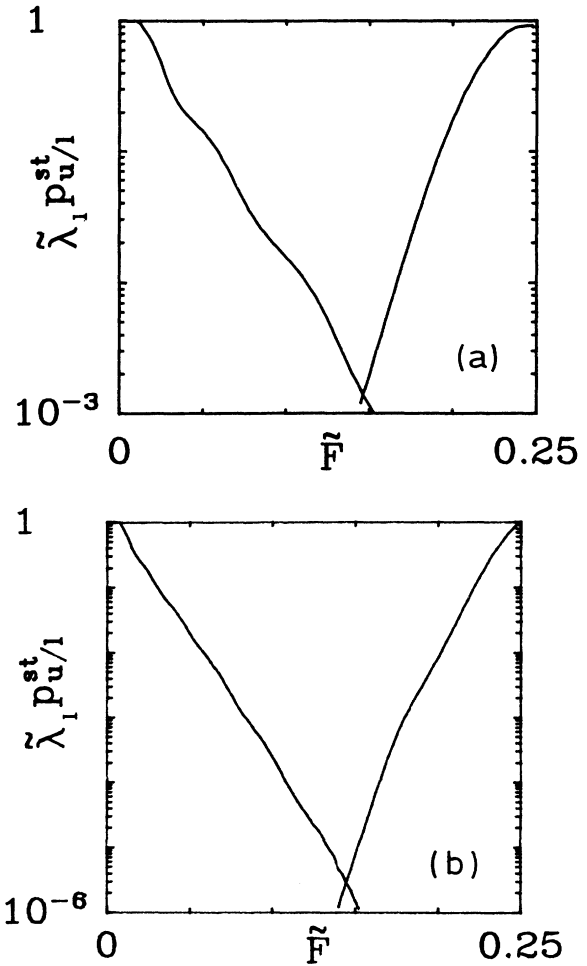

FIG. 11. Logarithmic plot of the eigenvalue $\tilde{\lambda}_1$ multiplied by p_u^{st} (right curve) or p_l^{st} (left curve), i.e., the transition rates from the lower to the upper branch or vice versa divided by 2κ, see (7.8). The parameters are the same as in Fig. 8.

Fig. 11. For driving fields well below (above) the transition field F_{tr} the transition rate from the upper (lower) branch to the lower (upper) one is much larger than the rate from the lower (upper) branch to the upper (lower) one. Well below and well above F_{tr} the transition rates $w(u \to l)$ and $w(l \to u)$ are connected to the first eigenvalue $\tilde{\lambda}_1$ by

$$w(u \to l) = 1/T(u \to l) = 2\kappa \tilde{\lambda}_1, \quad |F| < F_{tr}$$
$$w(l \to u) = 1/T(l \to u) = 2\kappa \tilde{\lambda}_1, \quad |F| > F_{tr} \ . \tag{7.10}$$

At the transition point F_{tr} both transition rates become equal and we have $(p_l^{st} = p_u^{st} = \frac{1}{2})$

$$w(u \to l) = w(l \to u) = \kappa \tilde{\lambda}_1, \quad |F| = F_{tr} \ . \tag{7.11}$$

Near the end of the bistability region, i.e., for $F \approx 0$ and $|F| \approx F_0$, the lowest nonzero eigenvalue is no longer much smaller than the other eigenvalues. In this case the concept of a tunneling process with the two tunneling times $T(u \to l)$ and $T(l \to u)$ breaks down.

The rates $w(u \to l)$, $w(l \to u)$ and therefore also the

times $T(u \rightarrow l)$, $T(l \rightarrow u)$ have approximately an exponential dependence on $F > 0$ in the bistable region

$$1/T(u \rightarrow l) = w(u \rightarrow l) \sim \exp(-aF) ,$$

$$1/T(l \rightarrow u) = w(l \rightarrow u) \sim \exp[-b(F_0 - F)] . \qquad (7.12)$$

However, small additional ripples occur for the tunneling rates as well as for the lowest nonzero eigenvalue as best seen in the left parts of Figs. 9(a) and 11(a). These ripples seem to be correlated with steplike change of the higher eigenvalues.

B. Discussion of the other eigenvalues

In the bistability region, where the first nonzero eigenvalue $\tilde{\lambda}_1$ becomes very small, the next eigenvalue takes over the value of $\tilde{\lambda}_1$ outside the bistability region. The third eigenvalue goes down in two steps to the value the first eigenvalue has outside the bistability region, leading to a nearly twofold degeneracy similar as it is the case for the eigenvalues $\lambda_0 = 0$ and λ_1. Similar features are observed for the higher eigenvalues. A similar steplike change has been observed in the bistability region for a classical Brownian motion of a particle in a tilted periodic potential, see Refs. 16 and 17 or Figs. 11.43a and 11.46 of Ref. 13.

Note added in proof. For absorptive optical bistability eigenvalues have also been calculated by Englund *et al.* [J. C. Englund, W. C. Schieve, W. Zurek, and R. F. Gragg, in *Optical Bistability*, edited by C. M. Bowden, M. Ciftan, and H. R. Robl (Plenum, New York, 1981)].

ACKNOWLEDGEMENT

APPENDIX: APPROXIMATE EXPRESSION FOR THE LOWEST EIGENVALUE

The Hamilton operator (2.3) is an Hermitian operator. Therefore the lowest eigenvalue and its eigenfunction ψ follow from the variational principle

$$E = \langle \psi | H | \psi \rangle / \langle \psi | \psi \rangle . \qquad (A1)$$

Using the coherent state

$$| \psi \rangle = | \alpha \rangle \qquad (A2)$$

as a trial function, we obtain

$$E_1 \leq f(\alpha) = -\Omega |\alpha|^2 + \chi |\alpha|^4 - F(\alpha + \alpha^*) . \qquad (A3)$$

The minimum value of $f(\alpha)$ is given by

$$\alpha = \alpha_u \qquad (A4)$$

where $\alpha_u = x_u^{st}$ is the upper branch in Fig. 1, compare (3.5) and (3.6). Using the normalization (3.8) we thus obtain

$$E_1 \leq f_{min} = f(\alpha_u) = (\Omega^2/\chi)(\tilde{x}_u^{st})^2[1 - 3(\tilde{x}_u^{st})^2] , \qquad (A5)$$

$$\tilde{F} = -\tilde{x}_u^{st} + 2(\tilde{x}_u^{st})^3 . \qquad (A6)$$

Elimination of $\tilde{x}_u^{st}$ leads approximately to the first eigenvalue $E_1(\tilde{F}) \approx f_{min}$. The other solution with $\partial f / \partial \alpha = 0$ leads to $\alpha = \alpha_l$ where $\alpha_l = \tilde{x}_l^{st}$ is the lower branch in Fig. 1. Replacing in (A5) and (A6) $\tilde{x}_u^{st}$ by $\tilde{x}_l^{st}$ then leads approximately to

$$E_{11}(\tilde{F}) \approx f(\alpha_l) ,$$
$$E_{20}(\tilde{F}) \approx f(\alpha_l) , \qquad (A7)$$

see Figs. 2(a) and 2(b), respectively. (Obviously no exact upper bound can be given in this case.) Calculating the variance of H for the stationary states $|\alpha_u\rangle$ and $|\alpha_l\rangle$ we obtain

$$\Delta H = \sqrt{2}\chi |\alpha_u|^2; \quad \Delta H = \sqrt{2}\chi |\alpha_l|^2 . \qquad (A8)$$

Thus the coherent states $|\alpha_u\rangle$ and $|\alpha_l\rangle$ are not exact eigenstates of H for $|\alpha_l|^2 > 0$ ($|\alpha_u|^2$ is always larger than zero). Because for small values of $|F|$, $|\alpha_l|^2$ is very small, $|\alpha_l\rangle$ is nearly an eigenstate of H for small $|F|$. For the lower branch the ratio $\Delta H / E$ is of the order $\sqrt{2}\chi/\Omega$ for small F whereas for the upper branch $\Delta H / E$ is of the order $(\sqrt{2}/3)(2\chi/F)^{2/3}$ for large F. Thus in the lower branch for small F and in the upper branch for large F $|\alpha_l\rangle$ and $|\alpha_u\rangle$ can be used as approximate eigenstates. For these eigenstates the matrix elements are given by

$$\langle \alpha_l | a | \alpha_l \rangle = x_l^{st}, \quad \langle \alpha_u | a | \alpha_u \rangle = x_u^{st} . \qquad (A9)$$

Because of

$$\langle \alpha_l | a^\dagger a | \alpha_l \rangle = |\langle \alpha_l | a | \alpha_l \rangle|^2 = x_l^{st2}$$

and

$$\langle \alpha_u | a^\dagger a | \alpha_u \rangle = |\langle \alpha_u | a | \alpha_u \rangle|^2 = x_u^{st2}$$

the master equation (5.6) has stationary solutions where only the occupation of one of these states is equal to one. For small F and large Ω/χ and for large F we thus obtain for $\langle a \rangle$ the classical result of the lower branch (small F) and of the upper branch (large F).

*Permanent address: Abteilung für Theoretische Physik I, Universität Ulm, D-7900 Ulm, Federal Republic of Germany.

†Permanent address: Fachbereich Physik, Gesamthochschule Essen, D-4300 Essen 1, Federal Republic of Germany.

[1]L. A. Lugiato, *Progress in Optics XXI*, edited by E. Wolf (North-Holland, Amsterdam, 1984) p. 69.

[2]H. A. Kramers, Physica **7**, 284 (1940).

[3]A. J. Leggett, Prog. Theor. Phys. (Suppl.) **69**, 80 (1980).

[4]A. O. Caldeira and A. J. Leggett, Phys. Rev. Lett. **46**, 211 (1981).

[5]U. Eckern, Nature **319**, 726 (1986).

[6]P. Hänggi, J. Stat. Phys. **42**, 105 (1986).

[7]J. M. Martinis, M. H. Devoret, and J. Clarke, Phys. Rev. Lett. **55**, 1543 (1985).

[8]A. Schenzle and H. Brand, Opt. Commun. **31**, 401 (1979).

[9]P. D. Drummond, Phys. Rev. A **33**, 4462 (1986).

[10]P. D. Drummond and D. F. Walls, J. Phys. A **13**, 725 (1980).

[11]C. W. Gardiner, *Handbook of Stochastic Methods,* Vol. 13 of *Springer Series in Synergetics,* 2nd ed. (Springer, Berlin, 1985).

[12]F. Haake, H. Risken, C. Savage, and D. F. Walls, Phys. Rev. A **34**, 3969 (1986).

[13]H. Risken, *The Fokker-Planck Equation,* Vol. 18 of *Springer Series in Synergetics* (Springer, Berlin, 1984).

[14]J. Keizer, *On the Solutions and the Steady States of a Master Equation* (Plenum, New York, 1972).

[15]P. D. Drummond, K. J. McNeil, and D. F. Walls, Opt. Acta **28**, 211 (1981).

[16]H. D. Vollmer and H. Risken, Z. Phys. B **52**, 259 (1983).

[17]P. Jung and H. Risken, Z. Phys. B **54**, 357 (1984).